



MERIS GLOBAL LAND SURFACE ALBEDO MAPS

Doc. ID : ATBD Cloud detection


Issue : 1 Rev.:0

Date : 10.02.2006

ATBD CLOUD DETECTION

Rene Preusker, Anja Hünerbein, Jürgen Fischer

**Institut für Weltraumwissenschaften
Freie Universität Berlin**

	MERIS GLOBAL LAND SURFACE ALBEDO MAPS	Doc. ID : ATBD Cloud detection Issue : 1 Rev.:0 Date : 25.04.2006 Page : ii
---	--	---

Internal Distribution

<u>Name</u>	<u>Quantity</u>
-------------	-----------------

External Distribution

<u>Name</u>	<u>Quantity</u>
-------------	-----------------

Change Record

<u>Issue</u>	<u>Revision</u>	<u>Date</u>	<u>Description</u>	<u>Change pages</u>
1	0	10.02.2006	First version	-


	MERIS GLOBAL LAND SURFACE ALBEDO MAPS	Doc. ID : ATBD Cloud detection Issue : 1 Rev.:0 Date : 25.04.2006 Page : iii
---	--	--

Table of Contents

1.	INTRODUCTION.....	1
1.1	PURPOSE	1
1.2	BACKGROUND.....	1
1.3	OBJECTIVES	1
1.3.1	<i>Improvement of the cloud detection</i>	1
1.3.2	<i>Likelihood of clouds</i>	2
2.	ALGORITHM OVERVIEW	2
3.	ALGORITHM DESCRIPTION	3
3.1	THEORETICAL DESCRIPTION	3
3.1.1	<i>Physics of the Problem</i>	3
3.1.2	<i>Spectral variability of channel 11</i>	4
3.2	MATHEMATICAL DESCRIPTION OF THE ALGORITHM	5
3.2.1	<i>Calculation of the inversion matrices</i>	5
3.2.2	<i>Data pre-processing</i>	8
3.2.3	<i>Cloud detection</i>	9
3.2.4	<i>Data post-processing</i>	10
3.3	PRACTICAL CONSIDERATIONS.....	10
3.3.1	<i>Numerical computation considerations</i>	10
3.3.2	<i>Calibration and Validation</i>	10
3.3.3	<i>Quality Control and Diagnostics</i>	10
3.3.4	<i>Exception Handling</i>	10
3.3.5	<i>Output Product</i>	10
4.	ERROR BUDGET ESTIMATES	10
5.	ASSUMPTIONS AND LIMITATIONS.....	11
6.	ABBREVIATIONS, SYMBOLS AND DEFINITIONS.....	11
7.	REFERENCES	11

List of Figures

Figure 1:	<i>Scheme of the cloud detection algorithm.</i>	3
Figure 2:	<i>Central wavelength of MERIS channel 11 as a function of it's across track position</i>	4
Figure 3:	<i>Measured likelihood of cloudiness (black) and fitted logistic function (green) for the land (left) and the open ocean (right) algorithm.</i>	8

List of tables

<i>Table 1: MERIS bands used in the proposed cloud detection algorithm.</i>	5
<i>Table 2: Important atmospheric and surface parameter used in the RT simulations.</i>	6
<i>Table 3: Composition of the training pattern.</i>	7
<i>Table 4: Limits of the input data.</i>	9

1. INTRODUCTION

1.1 Purpose

This Algorithm Theoretical Basis Document (ATBD) describes an algorithm to detect cloudy pixel in Level 1B data from the Medium Resolution Imaging Spectrometer (MERIS). The algorithm estimates for every pixel the likelihood of cloudiness. It has been developed in the frame of the Albedomap project, but it is a general applicable algorithm and part of the Basic ERS & Envisat, (A)ATSR and Meris (BEAM) toolbox.

1.2 Background

Although clouds are mostly easy to spot when a manual classification of satellite images is done, their automatic detection is difficult. Actually clouds have three radiative properties in the visible and infrared spectral range that enable their detection: 1.) clouds are white in the visible and near infrared, 2.) clouds are bright in the visible and near infrared and 3.) clouds are cold in the thermal infrared. Additionally water and ice clouds show some distinct extinction features at 1.6 μ m and 3 μ m.


But clouds, as the most variable atmospheric constituent, seldom show all properties at the same time. Thin clouds show a portion of the underlying surface spectral properties and low clouds are sometimes warmer than the ground. Additionally some surface types, like snow, ice and deserts have spectral properties that are similar to some of the clouds properties. Therefore simple threshold algorithms often fail and existing cloud detection schemes use a number of different cascaded threshold based tests to account for their complexity [Ackermann et al. 1998; King et al. 1992; Saunders and Kriebel 1988]. MERIS measures reflectance in 15 channels between 400nm and 1000nm. Thus the very valuable thermal information and the information from the liquid and ice water absorption are not available. The cloud detection for MERIS must therefore rely on the cloud brightness and "whiteness". In this way the cloud detection for MERIS has already been developed and is implemented in ESAs Level 2 scene identification [Santer et al. 1997].

1.3 Objectives

The algorithm described in this document is improving the cloud detection in two aspects. First, it is increasing the cloud detection selectivity compared to the standard level 2 scene identification. Second, it is delivering not only a binary cloud mask, but a likelihood of cloudiness, which is very valuable for succeeding algorithms.

1.3.1 Improvement of the cloud detection selectivity

The cloud detection selectivity is increased by using an additional information: the estimated main scattering height, which could be cloud tops or the surface. A height being significantly above the surface indicates the presence of a cloud layer. The cloud top height, or more precise the air mass above the cloud (the cloud top pressure), can be estimated using

	MERIS GLOBAL LAND SURFACE ALBEDO MAPS	Doc : ATBD Cloud detection Issue : 1 Rev : 0 Date : 25.04.2006 Page : 2
---	--	---

measurements in MERIS channel 11 at the oxygen A absorption band at 760nm [Fischer et al. 1997].

1.3.2 Estimation of the likelihood of cloudiness

In general cloud detection algorithms can be separated into two classes: clear sky conservative and cloud conservative. Clear sky conservative algorithms are constructed such that the probability of a first order error in clear sky detection is very low; in other words: if a pixel is detected as clear the probability of cloudiness should be very low. This has often the side effect that many cloud free pixel are detected as cloudy. The opposite is true for cloud conservative algorithms. Here the probability of a first order error in cloud detection is low, with the side effect that many cloudy pixels could be missed. This leads to two different nomenclatures. Pure clear sky conservative algorithms mark pixel as cloud free or as probably cloudy, whereas pure cloud conservative algorithms detect cloudy or probably cloud free pixel. However, in practice most cloud detection algorithms try to minimize the probability of the first and secondary order error in cloud and cloud free detection, only with the tendency to cloud or to clear sky conservative. What kind of cloud detection algorithm should be used is mainly a question of the succeeding algorithm. Algorithms relying on cloudy pixel need a cloud conservative cloud detection and vice versa, climatologically applications need balanced detections which are bias free.

The new algorithm is able to serve both needs. On the basis of extensive validation studies it returns for every pixel the likelihood of cloudiness. In this way cloud free conservative detection and cloud conservative detection needing algorithms can use their own threshold of probability of cloudiness.

2. ALGORITHM OVERVIEW

The cloud detection scheme described herein is designed for the MERIS Level1B data and is based on inverse modelling of radiative transfer simulations covering the natural variability of spectral cloud and surface properties. The simulated radiances have been used to train an artificial neural network (ANN) to discriminate between the cloudy and cloud free cases. During the validation of the network (up to now in a somehow incestuous way using the simulated data, in future with independent observations) the relation between a recall value of the ANN and the real likelihood of cloudiness is parameterized using a logistic function.

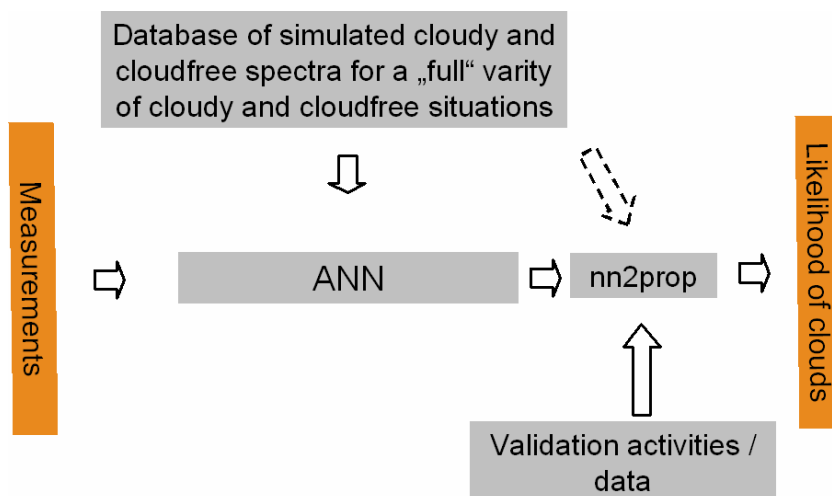


Figure 1: Scheme of the cloud detection algorithm.

An artificial neural network (ANN), trained with simulated radiances, converts MERIS measurements and the surface pressure into a number between 0 and 1. This number is finally converted into a likelihood of cloudiness. The latter conversion is based on data from validation activities.

3. ALGORITHM DESCRIPTION

3.1 Theoretical Description

The objective of the cloud detection scheme is to discriminate cloudy from cloud free pixel without using textural or temporal information; only spectral information is used: 1.) the top of atmosphere MERIS Level 1b reflectance, and 2.) the ratio between the reflectance at channel 11 at 760nm within the oxygen A absorption band and a reference channel at 754 nm (channel 10) together with the approximated surface pressure.

3.1.1 Physics of the Problem

Clouds consist of water droplets and ice particles with diameters between 0.1 μm and 100 μm , whereas the optical effective radius of cloud droplet distributions ranges typically from 5 μm to 40 μm , ice particle can be much bigger. The optical properties of such particle distributions, namely the spectral extinction and absorption, can be calculated using the Mie theory [Wiscombe, 1980] if the particles are spheres and using geometrical optics if the ice particles are large enough [Macke et al. 1996]. However, in all cases the extinction coefficient is spectrally neutral in the visible. Additionally water and ice show no or only a very small amount absorption in the visible spectral range, leading to a single scattering albedo of 1. These two optical properties correspond to the two most obvious features of clouds seen from space: they are white and bright. [[Figure [tb included] shows the spectral extinction coefficients and the single scattering albedo of several cloud particle distributions between 400nm and 1000nm.]]

Clouds have, compared to all other atmospheric constituents, very high optical thicknesses in the visible spectral range. Therefore clouds shield the surface from the solar radiation and the mean photon path in a cloudy atmosphere is usually shorter than in a cloud free atmosphere. The mean photon path length in a cloud free atmosphere can be estimated if the surface pressure and the surface brightness are known. Additionally, the actual mean photon path length can be deduced using measurements in the oxygen A absorption band at 760nm (which is covered by MERIS channel 11), whereas a low measured amount of absorption belongs to short photon paths and a high amount of absorption belongs to long paths. ESAs L2 cloud top pressure algorithm [Fischer et al. 1997] is using this information to estimate the air mass above a cloud or the surface. An inconsistency between the assumed clear sky surface pressure and the measured amount of absorption indicates the presence of a cloud.

The spectral and directional properties of cloud free open ocean pixel and land pixel differ significantly from each other. Open ocean pixel show a strong dependence of the spectrum on the viewing geometry: the sun glint region is bright and white, whereas the backscattered light is dominated by Rayleigh scattering (Figure to be included). Land pixels don't show such features. Tentative investigations have shown, that the results of the cloud detection are better if the algorithm is separated into two parts: one for the open ocean and one for the other pixel (henceforth called "land pixel").

3.1.2 Spectral variability of channel 11

MERIS is an imaging spectrometer consisting of 5 identical modules arranged in a fan shape configuration where each camera is covering a 14 degree field of view. The spectral dimension is achieved by imaging the entrance slit of the spectrometer via a dispersing grating onto a CCD array. This leads to small variations of the central wavelength of each band across the field of view of each module: the "smile effect". For MERIS the variability can reach 1.5nm (see Figure 2). All algorithms using bands close to strong spectral features need a precise spectral characterization, a single central wavelength is not sufficient. This is especially true for algorithms using band 11, including the herein described cloud detection.

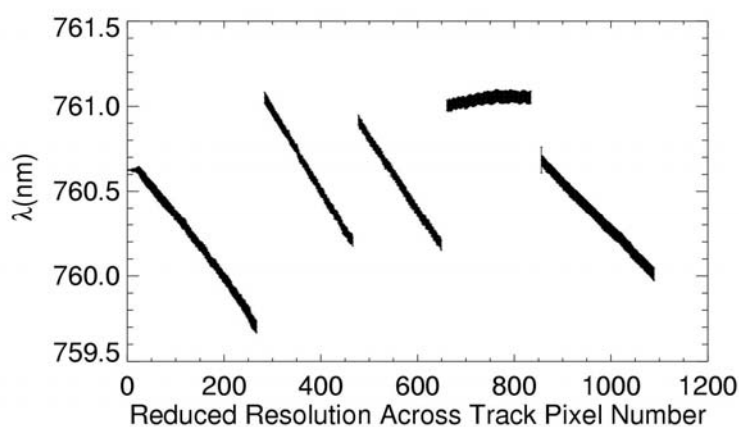


Figure 2: Central wavelength of MERIS ch. 11 as a function of it's across track position. Clearly visible are the 5 MERIS modules and the variability within each module ("smile effect")

3.2 Mathematical description of the algorithm

The inversion of the radiative transfer to detect cloudy pixel is performed by a special type of an artificial neural network: a Multi-layer Perceptron (MLP). The parameters of the MLP (henceforth called the inversion matrices) are found during an optimization process (the training) using the results of radiative transfer simulations. The usage of an MLP for the multidimensional non-linear regression of the simulated data to the cloudiness of a pixel has the disadvantage of not being physically based in a sense that the elementary functions of an MLP do not correspond to the radiative transfer in cloudy and cloud free atmospheres. Therefore the MLP will give un-predictable and un-physical answers if the input data is outside the data space of the training dataset. To minimize this disadvantage effort must be put into the thorough generation of the training dataset, into the pre-processing of the satellite data, which must filter out such data, and into the validation of the algorithm. On the other hand the usage of an MLP has the advantage of optimizing the needed coefficients in an objective and comprehensive way by minimizing a cost function, in contrast to the common procedure of manually adapting and combining thresholds.

The first part of this section describes the radiative transfer simulations and the calculation of the inversion matrices. The second part describes the application of the found inversion matrices to MERIS data to estimate the likelihood of clouds.

It is beyond the bounds of this document to list all calculated weight matrices, parameter and scaling factors, but they can be found in the ".../auxdata/cloud/" directory of the beam installation.

3.2.1 Calculation of the inversion matrices

3.2.1.1 Radiative transfer simulations

Radiative transfer simulations have been performed to create a comprehensive data set as a basis for the MLP training. We used the radiative transfer model MOMO based on the Matrix-Operator-Method [Fischer and Grassl, 1984; Fell and Fischer, 2001], to create the database. It is a one dimensional model generating azimuthally resolved reflectances at TOA for the used MERIS bands (**Table 1**) for a variety of observation and illumination geometries. The simulations cover the whole range of possible cloudy and cloud free conditions. The spectral properties of the surface range from dark ocean surfaces to white snow covered surfaces, the surface heights range from pressures of 1100hPa to 250hPa. The clouds have optical thicknesses between 0.5 and 150 and heights between 30hPa and 800 hPa above the ground. (**Table 2**)

(MERIS band)	(01) 412,50	(02) 442,50	(03) 490,00	(04) 510,00
wavelength	(05) 560,00	(06) 620,00	(09) 708,75	(10) 753,75
[nm]	(11) 760,10 (*)	(13) 865,00		

Table 1: MERIS bands used in the proposed cloud detection algorithm.

(*)Channel 11 has been simulated for several central wavelengths in the range [759.nm, 763nm] to account for the smile effect.

Parameter	Range
Cloud optical thickness (0)	0., 0.5, 1., 2., 5., 10., 20., 40., 80., 150.
Surface type (1)	ocean 2m/s, ocean 7m/s, dessert, sparse vegetation, dense vegetation, snow, urban
Surface height (2)	-100m , 0, 500m, 1200m, 2500m, 4500m, 8900m
Cloud top height (3)	700m, 1500m, 2500m, 2700m, 5000m, 7000m, 9000m, 11000m, 16000m

Table 2: Important atmospheric and surface parameter used in the RT simulations.

(0) A cloud optical thickness of 0 is the “cloud free case”. (1) The BRDF of the ocean surface is calculated according to a wind speed of 2m/s and 7m/s, the spectral properties of the land surfaces are calculated using NASAs “Aster spectral library” [Nasa]. (2)The surface height is given relative to the sea level.(3) Not all combinations of cloud top height and surface heights have been used, clouds were always at least 30hPa higher than the ground

3.2.1.2 Azimuth different definition

According to the ESA practice, an azimuth difference of 180° is assigned to the forward scattering direction (e.g. the sun glint) while a difference of 0° is assigned to the backscattering direction.

3.2.1.3 Observer geometry transformation

The observer geometry needs to be transformed into Cartesian coordinates to avoid discontinuities of the azimuth difference at Nadir. The parameters x and z are used as input to the network.

$$\begin{aligned}x &= \sin(\vartheta_{\text{view}}) \cos(\phi_{\text{azi}}) \\y &= \sin(\vartheta_{\text{view}}) \sin(\phi_{\text{azi}}) \\z &= \cos(\vartheta_{\text{view}})\end{aligned}$$

The parameter y can be calculated from x and z and is therefore not needed as an extra information for the algorithm.

3.2.1.4 Composition of the training pattern

Each training pattern consists of an input and an output vector. The input vector I contains all information used later on for the cloud detection: the absorption free MERIS Level1b reflectances, the reflectance ratio of channel 11 and channel 10, the associated wavelength λ of channel 11, the cosine of the solar zenith, the cosine of the viewing zenith, the transformed azimuth difference (x) and the surface pressure p . The output vector consists of only one number: the cloud mask cm (0 is cloud free, 1 is cloudy). Herein the reflectance ρ is defined as:

$$\rho(\lambda) = \frac{L(\lambda)}{F_0(\lambda) \cdot \cos(\vartheta_{\text{sol}})},$$

where $F_0(\lambda)$ is the solar irradiance and $L(\lambda)$ is the measured TOA radiance.

Training pattern	(01) ρ_{412}	(02) ρ_{442}	(03) ρ_{490}	(04) ρ_{510}
	(05) ρ_{560}	(06) ρ_{620}	(07) ρ_{708}	(08) ρ_{754}
	(09) ρ_{865}	(10) ρ_{761}/ρ_{754}	(11) p	(12) $\lambda(\text{ch11})$
	(13) $\cos(\mathcal{G}_{\text{sol}})$	(14) $\cos(\mathcal{G}_{\text{view}})$	(15) x	(16) cm

Table 3: Composition of the training pattern.

The first 15 elements are the input vector; the last element is the (one-dimensional) output vector, the cloud mask.

3.2.1.5 Optimization / Training

Formally, the signal processing in an MLP can be written as:

$$\tilde{O} = \sigma(W_n \# \sigma(\dots(W_2 \# \sigma(W_1 \# \tilde{I}))\dots))$$

An input vector I is transformed into an output vector O by a sequence of multi-dimensional linear transformations and non-linear scalings (the swung dash indicates that the input and the output vector are usually pre-processed, for instance scaled to values between 0 and 1. But this pre-processing is fixed and not part of the training). The linear transformation is a matrix multiplication with W_i denoted by $\#$. The non-linear scaling is the element wise application of the non-linear function σ to the result i of each linear transformation.

$$\sigma_i(i) = \frac{1}{1 + e^{-i}}$$

The used MLP has three layers and therewith two weight matrices W_1 and W_2 . The objective of the training is to find the matrices W_1 and W_2 that minimize the cost function L .

$$L(W_1, W_2) = \frac{1}{n} \sum_{i=1}^n \sum_{j=1}^m (O^{i,j}_{sim} - O^{i,j}_{net}(W_1, W_2))^2 \Rightarrow \min$$

O_{net} is the output vector from the MLP and O_{sim} is the output vector from the simulation. n is the number of training pattern, m is the number of elements of the output (in our case 1). Several methods can be utilized for the optimization; here a gradient descent optimization has been used.

3.2.1.6 Parameterisation of the Likelihood of Cloudiness

During the validation of the network the relation between a recall value o of the MLP and the likelihood of cloudiness $P(o)$ will be quantified:

$$P(o_a, o_b) = \frac{n(o_a, o_b)}{N(o_a, o_b)}$$

N is total number of cases where the recall of the ANN is between o_a and o_b , n is the number of cloudy pixel among them. These types of probability distributions of quasi *dichotomous* variables can be approximated by a two parameter logistic function:

$$P(o) = \frac{1}{1 + \exp(-\tau \cdot (o - x_m))}$$

Up to now the parameter τ and x_m are approximated using simulated data. In future it will be based on independents validation data. Further future enhancement could be situation dependent parameter sets of τ and x_m (depending on season, underlying surface). **Figure 3** shows the current probability distributions and the fitted logistic functions for the land and the sea algorithm.

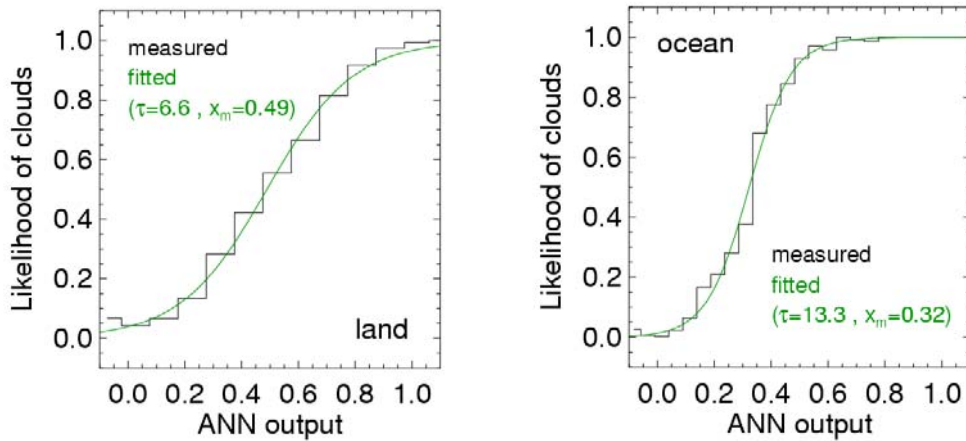


Figure 3: Measured likelihood of cloudiness (black) and fitted logistic function (green) for the land (left) and the open ocean (right) algorithm.

3.2.2 Data pre-processing

3.2.2.1 Actual surface pressure

MERIS L1b data contains 1.) the surface pressure p_s for sea level from the European Centre for Medium-Range Weather Forecasts (ECMWF) and 2.) the surface height h from a digital elevation model (DEM) at the tie points. 1.) and 2.) are bi-linear interpolated to the respective pixel position and the actual surface pressure is estimated using the *international barometric formula for a standard atmosphere* [Zitat??]:

$$p(h) = 1013.25 \cdot \left(1 - \frac{0.0065 \cdot h}{288.15}\right)^{5.255}$$

This is of course only an approximation but precise enough compared to most cloud top pressures, which are much higher than 30 hPa above the ground. Clouds close to the ground or fog will lead to ambiguities. This has to be investigated in more detail. Additionally the

consequence of the reduced spatial resolution of the assumed surface pressure at the tie points should be investigated. Further improvements should use more appropriate profiles.

3.2.2.2 Separation of open ocean pixel

Sea pixels are considered as Open Ocean if the ocean is deeper than 50m. The L1B digital elevation model data at the tie points is bi-linear interpolated to the respective pixel position. Further improvements could use a better DEM from auxiliary data.

3.2.2.3 Limit checks

The cloud detection algorithm produces reliable results only if all input data are within the training data space. Up to now a simple check is performed, which tests if all elements of the input vector are within its limits (**Table 4**). Data outside the limits will not be processed.

Parameter	Land		Open ocean	
	Minimum	Maximum	Minimum	Maximum
ρ_{412}	3.44e-02	3.76e-01	6.30e-02	3.48e-01
ρ_{442}	2.89e-02	4.16e-01	4.93e-02	3.48e-01
ρ_{490}	2.18e-02	4.60e-01	2.90e-02	3.46e-01
ρ_{510}	1.90e-02	4.62e-01	2.19e-02	3.45e-01
ρ_{560}	1.29e-02	4.48e-01	1.49e-02	3.46e-01
ρ_{620}	8.20e-03	4.66e-01	1.00e-02	3.49e-01
ρ_{708}	4.94e-03	5.65e-01	6.65e-03	3.53e-01
ρ_{754}	4.08e-03	5.93e-01	5.62e-03	3.55e-01
ρ_{865}	2.50e-03	6.10e-01	4.83e-03	3.59e-01
ρ_{761}/ρ_{754}	1.16e-01	9.92e-01	1.39e-01	9.93e-01
P	332 hPa	1025 hPa	980 hPa	1025 hPa
$\lambda(\text{ch11})$	759.0 nm	764.6 nm	759.0 nm	764.6 nm
$\cos(\vartheta_{\text{sol}})$	0.149	0.975	0.149	0.975
$\cos(\vartheta_{\text{view}})$	0.75	1.00	0.75	1.00
X	-0.661	0.661	-0.661	0.661

Table 4: Limits of the input data.

Further improvements will use a more sophisticated input data check, since this test is weak, if some elements of the input data are correlated (like the blue and the NIR reflectances).

3.2.3 Cloud detection

The cloud detection is straight forward. First, the input vector I has to be assembled for each pixel as described in **Table 3**. Second, the scaled input vector \tilde{I} has to be processed using:

$$o = \sigma(W_2 \# \sigma(W_1 \# \tilde{I}))$$

3.2.4 Data post-processing

The recall o has finally to be converted into a likelihood of cloudiness $P(o)$ using the parameter τ and x_m found during the validation.

$$P(o) = \frac{1}{1 + \exp(-\tau \cdot (o - x_m))}$$

3.3 Practical Considerations

Numerical exceptions (underflows (TBC) and overflows) have to be caught and flagged.

3.3.1 Numerical Computation Considerations

The algorithm needs no iterations and no searching. It is therefore save in operational applications.

3.3.2 Calibration and Validation

The validation of the cloud detection is an integral part of the algorithm. Without the validation the estimation of the probability of cloudiness can not be performed. However, this has not yet been done and will be the main task of future work

3.3.3 Quality Control and Diagnostics

3.3.4 Exception Handling

If the input vector is outside the training data space or if numerical exception occur, then the cloud probability of the pixel is set to corresponding “no data” value.

3.3.5 Output Product

Output product of the cloud detection algorithm is the likelihood of cloudiness of a pixel.

4. ERROR BUDGET ESTIMATES

The validation of the cloud detection is an integral part of the algorithm. Without the validation the proper estimation of the probability of cloudiness can not be performed. This has not yet been done and will be the main task of future work. The effect of fractional cloud cover has to be investigated.

5. ASSUMPTIONS AND LIMITATIONS

MERIS has not been designed for cloud remote sensing and lacks of thermal and NIR channels important for cloud detection and cloud/snow discrimination. Especially 1.) some thin high clouds (cirrus) will be invisible for MERIS and 2.) very low clouds and fog can not differentiated from snow.

Three dimensional effects, especially very heterogeneous low level clouds could lead to photon path extensions, which could be misinterpreted as cloud free situations.

6. ABBREVIATIONS, SYMBOLS AND DEFINITIONS

AER	Aerosol
ANN	Artificial neural network
ATBD	Algorithm theoretical basis document
BIAS	Bias (numerical offset)
ECMWF	European Centre for Medium-Range Weather Forecasts
DEM	Digital elevation model
Envisat	European environmental satellite
ESA	European Space Agency
L1b	Level1b
L2	Level2
MERIS	Medium Resolution Imaging Spectrometer
MLP	Multi-Layer Perceptron
MOMO	Matrix-Operator Model
NIR	Near-infrared
TOA	Top-Of-Atmosphere
VIS	Visible

7. REFERENCES

- Ackerman, Strabala, Menzel, Frey, Moeller, Gumley, Baum, Schaaf, & Riggs, 2002:** *Discriminating Clear-Sky from Cloud with MODIS - Algorithm Theoretical Basis Document.*
- Delwart S., R.Preusker, L. Bourg, R. Santer,D. Ramon, J. Fischer 2005,** MERIS in-flight spectral calibration, *International Journal of Remote Sensing*, in press
- Fell F., and J. Fischer,** Numerical simulation of the light field in the atmosphere-ocean system using the matrix-operator method", *Journal of Quantitative Spectroscopy & Radiative Transfer*, 69, 351-388, 2001.

Fischer J., and H. Grassl, Radiative transfer in an atmosphere-ocean system: an azimuthally dependent matrix-operator approach, *Applied Optics*, 23, 1032-1039, 1984.

Fischer J., R. Preusker, and L. Schueller. *ATBD cloud top pressure*. Algorithm Theoretical Basis Document PO-TN- MEL-GS-0006, European Space Agency, 1997.

King, M. D., Y. J. Kaufman, W. P. Menzel, and D. Tanré, 1992: Remote Sensing of Cloud, Aerosol, and Water Vapor Properties from the Moderate Resolution Imaging Spectrometer (MODIS). *IEEE Transactions On Geoscience and Remote Sensing*, 30, 1-27.

Hall, D.K., Riggs, G.A. and Salomonson V.V. 1995. Development of methods for mapping global snow cover using moderate resolution imaging spectroradiometer data, *Remote Sensing of Environment*, 54. pp. 127-140

Macke, A., J. Mueller, and E. Raschke 1996. Single scattering properties of atmospheric ice crystals. *J. Atmos. Sci.* 52, 2813-2825.

NASA, ASTER spectral library, URL:<http://speclib.jpl.nasa.gov/>, status March 2005

Rummelhart D. and J. McClelland, *Parallel Distributed Processing*, MIT Press, Cambridge, Massachusetts, 1986.

Santer R., Carrre V., Dessailly D., Dubuisson P., and Roger J.C. *ATBD pixel identification*. Algorithm Theoretical Basis Document PO-TN-MEL-GS-0005, European Space Agency, 1997.

Saunders, R. W. and R. T. Kriebel, An improved method for detecting clear sky and cloudy radiances from AVHRR data, *Int. J. Remote Sensing*, 9, 123 - 150, 1988

Wiscombe, W. J., Improved Mie scattering algorithm, *Applied Optics*, 19, 15505-1515, 1980.